Harvesting entropy and quantifying the transition from noise to chaos in a photon-counting feedback loop

Aaron Morgan Hagerstrom[a,b,1], Thomas Edward Murphy[a,c], and Rajarshi Roy[a,b,d]

[a]Institute for Research in Electronics and Applied Physics, University of Maryland, College Park, MD 20742; [b]Department of Physics, University of Maryland, College Park, MD 20742; [c]Department of Electrical and Computer Engineering, University of Maryland, College Park, MD 20742; and [d]Institute for Physical Science and Technology, University of Maryland, College Park, MD 20742

Edited by Katepalli R. Sreenivasan, New York University, New York, NY, and approved June 23, 2015 (received for review April 3, 2015)

Many physical processes, including the intensity fluctuations of a chaotic laser, the detection of single photons, and the Brownian motion of a microscopic particle in a fluid are unpredictable, at least on long timescales. This unpredictability can be due to a variety of physical mechanisms, but it is quantified by an entropy rate. This rate, which describes how quickly a system produces new and random information, is fundamentally important in statistical mechanics and practically important for random number generation. We experimentally study entropy generation and the emergence of deterministic chaotic dynamics from discrete noise in a system that applies feedback to a weak optical signal at the single-photon level. We show that the dynamics transition from shot noise to chaos as the photon rate increases and that the entropy rate can reflect either the deterministic or noisy aspects of the system depending on the sampling rate and resolution.

entropy | chaos | nonlinear dynamics | photon counting | statistical physics

Continuous variables and dynamical equations are often used to model systems whose time evolution is composed of discrete events occurring at random times. Examples include the flow of ions across cell membranes (1), the dynamics of large populations of neurons (2), the birth and death of individuals in a population (3), traffic flow on roads (4), the trading of securities in financial markets (5, 6), infection and transmission of disease (7), and the emission and detection of photons (8). We can identify two sources of unpredictability in these systems: the noise associated with the underlying random occurrences that comprise these signals, which are often described by a Poisson process, and the macroscopic dynamics of the system, which may be chaotic. When both effects are present, the macroscopic dynamics can alter the statistics of the noise, and the small-scale noise can in turn feed the large-scale dynamics. This can lead to subtle and nontrivial effects including stochastic resonance and coherence resonance (9, 10). Dynamical unpredictability and complexity are quantified by Lyapunov exponents and dimensionality, whereas shot noise is characterized by statistical metrics like average rate, variance, and signal-to-noise ratio. Characterizing the unpredictability of a system with both large-scale dynamics and small-scale shot noise remains an important challenge in many disciplines including statistical mechanics and information security.

Many cryptographic applications, including public key encryption (11), use random numbers. Because the unpredictability of these numbers is essential, physical processes are sometimes used as a source of random numbers (12–25). Physical random number generators are usually tested using the National Institute of Standards and Technology (26) and Diehard (27) test suites, which assess their ability to produce bits that are free of bias and correlation. These tests are an excellent assessment of the performance of a physical random number generator in practical situations but leave an important and fundamental problem unaddressed. Deterministic postprocessing procedures, such as hash functions (25), are often used to remove bias and correlation. Because these procedures are algorithmic and reproducible, they cannot in principle increase the entropy rate of a bit stream. Thus, the reliability of a physical random number generator depends on an accurate assessment of the entropy rate of physical process that generated the numbers (28). It remains difficult to assess the unpredictability of a system based on physical principles.

Evaluation of entropy rates from an information-theoretic perspective is also centrally important in statistical mechanics (29–36). One might expect that the unpredictability of a system with both small-scale shot noise and large-scale chaotic dynamics would depend on the scale at which it is observed. In many systems, the dependence of the entropy rate on the resolution, ε, and the sampling interval, τ, can reflect the physical origin of unpredictability (37–40). This dependence has been studied experimentally in Brownian motion, RC circuits, and Rayleigh–Bénard convection (34, 35, 37, 41, 42).

Here, we present an experimental exploration and numerical model of entropy production in a photon-counting optoelectronic feedback oscillator. Optoelectronic feedback loops that use analog detectors and macroscopic optical signals produce rich dynamics whose timescales and dimensionality are highly tunable (43–47). Our system applies optoelectronic feedback to a weak optical signal that is measured by a photon-counting detector. The dynamic range of this system (eight orders of magnitude in timescale and a factor of 256 in photon rate) allows us to directly observe the transition from shot noise-dominated behavior to a low-dimensional chaotic attractor with increasing optical power—a transition that, to our knowledge, has never been observed experimentally. We show that the entropy rate can reflect either the deterministic or stochastic aspects of the system, depending on the sampling rate and measurement resolution, and describe the importance of this observation for physical random number generation.

Significance

The unpredictability of physical systems can depend on the scale at which they are observed. For example, single photons incident on a detector arrive at random times, but slow intensity variations can be observed by counting many photons over large time windows. We describe an experiment in which we modulate a weak optical signal using feedback from a single-photon detector. We quantitatively demonstrate a transition from single-photon shot noise to deterministic chaos. Furthermore, we show that measurements of the entropy rate of a system with small-scale noise and large-scale deterministic fluctuations can resolve both behaviors. We describe how quantifying entropy production can be used to evaluate physical random number generators.

Author contributions: A.M.H., T.E.M., and R.R. designed research; A.M.H. performed research; A.M.H. analyzed data; and A.M.H., T.E.M., and R.R. wrote the paper.

The authors declare no conflict of interest.

This article is a PNAS Direct Submission.

[1]To whom correspondence should be addressed. Email: aaron.hagerstrom@gmail.com.

www.pnas.org/cgi/doi/10.1073/pnas.1506600112

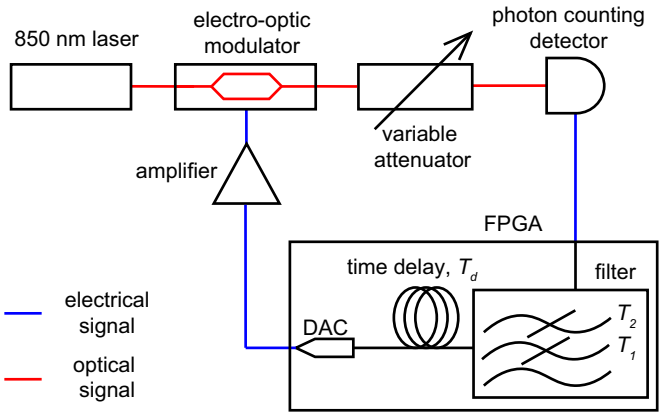

Fig. 1. Experimental configuration. We use a silicon avalanche photodiode, which detects individual photon arrivals. This signal is time-delayed and filtered using an FPGA, and the output of the filter drives the modulator, which in turn varies the light incident on the detector, forming a feedback loop.

Experiment and Results

Fig. 1 shows a schematic of our experimental configuration. Our system has a similar architecture to earlier experiments involving optoelectronic feedback loops but differs in that we use a photon-counting detector, whereas previous experiments used an analog photodetector. In either case, the signal from the detector is time-delayed and filtered, and the output of the filter drives the Mach–Zehnder electrooptic modulator (MZM), which in turn controls the light incident on the detector, forming a feedback loop. When an analog photodiode is used, the feedback loop is modeled by a time-delayed nonlinear differential equation:

$$\frac{d\boldsymbol{x}}{dt} = \boldsymbol{E}\boldsymbol{x} + \beta \boldsymbol{F} I(t),$$
$$I(t) = \sin^2\left[\boldsymbol{G}^T \boldsymbol{x}(t - T_d) + \phi\right]. \qquad [1]$$

Here, $\boldsymbol{x}$ is the state variable of a linear, time-invariant filter, matrix $\boldsymbol{E}$ and the vectors $\boldsymbol{F}$ and $\boldsymbol{G}$ describe the characteristics of the filter, $I(t)$ is the normalized intensity of light transmitted through the MZM, and T_d is the time delay. When a photon-counting detector is used in place of an analog photodiode, the filter variables can be modeled by a linear differential equation driven by discrete photon arrivals. In our implementation, the equations of motion for the filter variables are as follows:

$$\frac{d}{dt}\begin{pmatrix} x_1 \\ x_2 \end{pmatrix} = \begin{pmatrix} -\frac{1}{T_1} & 0 \\ 0 & -\frac{1}{T_2} \end{pmatrix}\begin{pmatrix} x_1 \\ x_2 \end{pmatrix} + \beta \begin{pmatrix} 1 \\ 1 \end{pmatrix} \frac{1}{\lambda_0} \sum_{i=1}^{\infty} \delta(t - t_i), \qquad [2]$$

where the photon arrivals times, $\{t_i\}$, are generated by a nonstationary Poisson point process whose rate, $\lambda(t)$, depends on the state of the filter variables:

$$\lambda(t) = \lambda_0 I(t) = \lambda_0 \sin^2[x_1(t - T_d) - x_2(t - T_d) + \phi]. \qquad [3]$$

In the limit that the λ_0 is large, the stochastic term in Eq. **2** can be replaced with its expectation value, $I(t)$, leading to Eq. **1**.

In our implementation, the time delay is T_d = 1.734 ms, the modulator bias is $\phi = \pi/4$, and the filter constants T_1 = 1.2 ms, and T_2 = 60 μs. The filter and time delay are implemented digitally using an Altera Cyclone II field programmable gate array (FPGA) and a digital-to-analog converter (DAC). The clock speed of this device is 151.1515 MHz, and we record all of the photon arrival times to this precision. The light source in our experiment is a continuous-wave fiber-coupled distributed feedback laser with a wavelength of 850 nm. Our detector has a dark count rate of ~ 100 cps and a dead time of about 100 ns. We vary the photon rate over a factor of 256, from $\lambda_0 T_d = 12.5$ (7.20×10^3 cps) to $\lambda_0 T_d = 3{,}200$ (1.845×10^6 cps). In all of the experiments shown here, β is kept constant at 8.87.

Fig. 2 shows several time series recorded with this system with increasing photon rate, showing a transition from Poisson noise to deterministic chaos. We plot $N_w(t)$, the number of photon arrivals in the interval $[t-w,t]$. In Fig. 2, all of the plots were generated with $w = T_d/4$. When the incident photon rate is $\lambda_0 T_d = 12.5$, the photons appear to arrive at random, uncorrelated times as in a stationary Poisson process. Increasing the incident photon rate to $\lambda_0 T_d = 200$, a smooth modulation of the photon rate starts to become apparent. At $\lambda_0 T_d = 3{,}200$, $N_w(t)$ has a smooth character and qualitatively resembles a low-dimensional chaotic signal. We also plot the results of a deterministic simulation using Eq. **1**. This time series was smoothed with a moving average over a time window of width w to be directly comparable with $N_w(t)$. We plot the autocorrelation function, $C(t') = \langle (N_w(t) - \overline{N_w})(N_w(t - t') - \overline{N_w}) \rangle$, normalized so that the value of the autocorrelation function is unity at $t' = 0$. As the photon rate increases from $\lambda_0 T_d = 12.5$, the autocorrelation function changes from a δ-like peak, characteristic of a Poisson process, to an oscillatory function that shows correlations at long timescales (tens of milliseconds). The autocorrelation function of the deterministic simulation time series is in close agreement with the autocorrelation function of the photon arrivals with $\lambda_0 T_d = 3200$. Histograms of $N_w(t)$ also show a transition from a nearly Poisson distribution to a bimodal distribution characteristic of the deterministic chaotic process.

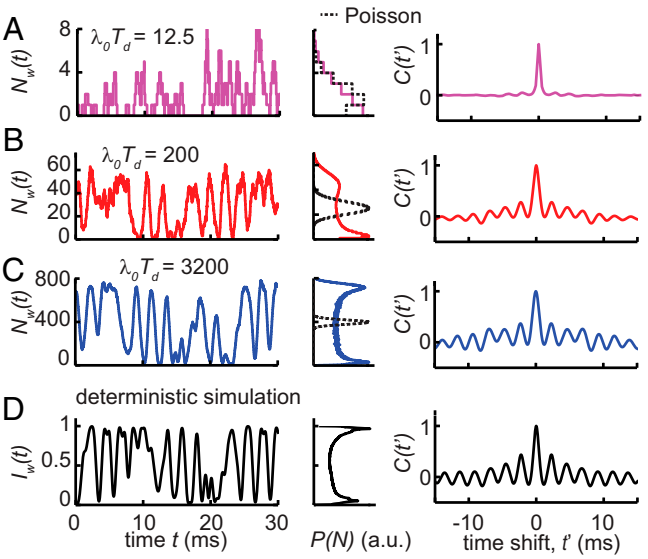

Fig. 2. Time series, probability distributions, and autocorrelation functions. *A–C* show experimental data, and *D* shows the result of a deterministic simulation of Eq. **1**. (*A*) At a low photon rate of $\lambda_0 T_d = 12.5$, the dynamics appear Poissonian. The time series has no visible structure, the autocorrelation function is sharply peaked at 0, and the distribution of photon counts in a window of $w = T_{d/4}$ is nearly Poisson. (*B*) $\lambda_0 T_d = 200$, a slow modulation of the photon rate is evident. (*C*) At $\lambda_0 T_d$ = 3,200, the photon rate varies smoothly, the photon count distribution is bimodal and much wider than a Poisson distribution with the same mean, and the autocorrelation function shows slow oscillations. The deterministic simulation *D* shows the same features as the high photon rate data shown in *C*.

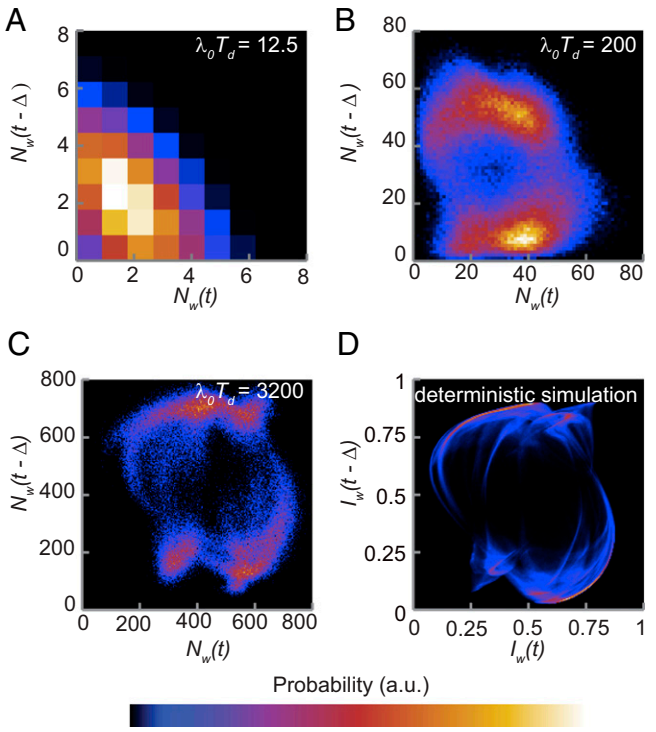

Fig. 3. Poincaré sections. We visualize the emergence of a chaotic attractor from Poisson noise with increasing photon rate by embedding photon count time series in two dimensions with a time delay of $\Delta = T_d/4$, and reducing the dimensionality of the dynamics by plotting points only when the state of the system in phase space passes through a codimension 1 surface defined by $x_1 - x_2 = \pi$. *A–C* show experimental data, and *D* shows the result of a deterministic simulation. These histograms are constructed with a bin width of one photon in *A* and *B*, four photons in *C*, and 0.005 in *D*.

To visualize the development of chaos with increasing photon rate, we show Poincaré surfaces of section in Fig. 3. We perform a time delay embedding of the experimental time series $N_w(t)$, using a time delay of $\Delta = T_d/4$, by constructing a list of points in 2D space of the form $[N_w(t), N_w(t-\Delta)]$. Because the attractor has a dimension higher than 2, we reduce the dimensionality of the attractor by plotting the points only when the state variables pass through a codimension 1 Poincaré surface defined by $x_1 - x_2 = \pi$. The embeddings show a similar trend to the plots in Fig. 2. We see a development of complex chaotic dynamics from discrete photon noise as the photon rate increases. The deterministic simulation is plotted for comparison, and, as in Fig. 2, a moving average of width w is used so that the smoothed intensity time series, $I_w(t)$, is directly analogous to $N_w(t)$. The deterministic signal in Fig. 3*D* can be regarded as the infinite photon rate limit of the photon-counting system.

Fig. 4 shows the dependence of the variance of N_w on the window w and offers another indication of the transition from shot noise to deterministic chaos. The time integral of an uncorrelated random signal executes a random walk in which the variance grows linearly with the integration time. For this reason, we plot $\mathrm{Var}(N_w)/w$ in Fig. 4. We see distinct asymptotic growth rates of the variance with small and large w. When w is small, the variance reflects the Poissonian nature of the photon arrivals, and the growth rate of the variance has roughly constant value of $\mathrm{Var}(N_w)/w = \lambda_0 \bar{I}$. In the limit where the counting window is much longer than the timescale of the variations in intensity, $N_w(t)$ can be regarded as the sum of the photon counts in many independent identically distributed intervals, and the central limit theorem implies that the variance will grow in proportion to w.

As we increase the photon rate from $\lambda_0 T_d = 12.5$ to $\lambda_0 T_d = 3{,}200$, we see an increasing offset between the two asymptotic rates of growth of the variance. The variance can be related to the photon rate, counting window, and the unnormalized autocorrelation function, $c_I(t') = \langle (I(t) - \bar{I})(I(t-t') - \bar{I}) \rangle$ (Eq. **4** is found in section 14.9.2 of ref. 8):

$$\mathrm{Var}(N_w) = w \left[\lambda_0 \bar{I} + \lambda_0^2 \underbrace{\int_{-w}^{w} dt' \left(1 - \frac{|t'|}{w}\right) c_I(t')}_{\Theta(w)} \right]. \qquad [4]$$

The second term in Eq. **4** accounts for the difference between the observed variance and the variance of a Poisson process with the same rate. The quantity $\Theta(w)$ has units of time and measures the correlations in $I(t)$ introduced by the feedback. This quantity increases from 0 to an asymptotic value Θ_∞ as w increases, accounting for the shape of the curves shown in Fig. 4. In deterministic simulations, we find $\Theta_\infty = 150$ μs. The value of Θ_∞ is related to the size of the intensity fluctuations, and the rate at which $\Theta(w)$ approaches this asymptotic value is determined by the timescales of the correlations of $I(t)$.

We characterize the entropy production using the (ε, τ) entropy per unit time, $h(\varepsilon, \tau)$ (37). This measurement of entropy has two parameters: sample resolution, ε, and sampling time interval, τ, which are natural parameters for most experiments because measurement devices record data to finite resolution at discrete times. In addition to being experimentally relevant, the dependence of $h(\varepsilon, \tau)$ on these parameters can reflect the underlying physical origin of unpredictability (37, 39, 40).

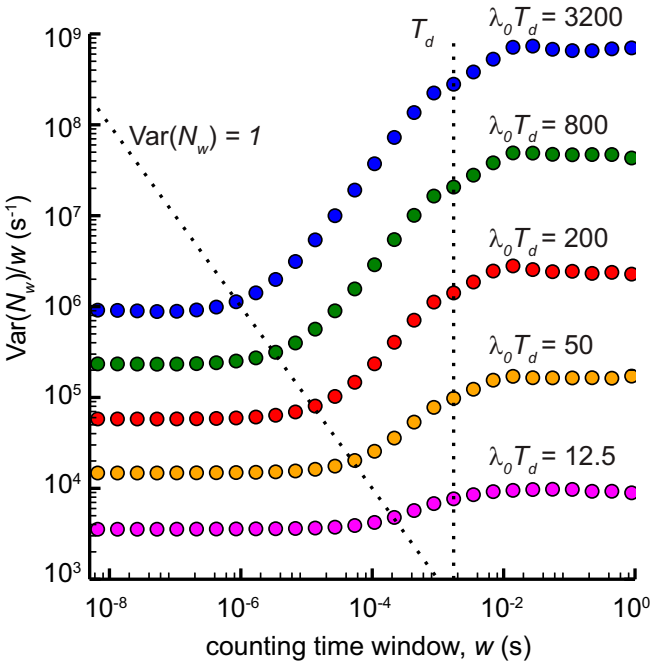

Fig. 4. Experimental dependence of growth rate of variance on counting time window, w. To indicate the timescale of the deterministic dynamics we indicate T_d. We also show a line indicating $\mathrm{Var}(N_w) = 1$, which roughly separates timescales over which less than one photon arrives in the counting window from timescales over which many photons arrive. Distinct asymptotic values of $\mathrm{Var}(N_w)/w$ are seen in the limits of small and large w. The offset between these two values reflects deterministic correlations in the photon arrival rate and grows with increasing photon rate.

In chaotic systems, unpredictability is due to the sensitive dependence on initial conditions. Because small perturbations grow exponentially in time, chaotic systems generate information. The growth of uncertainty is quantified by the Lyapunov exponents, μ_i, and in particular the largest exponent, μ_1. Positive Lyapunov exponents and entropy rate both quantify unpredictability, and there is a close relationship between these two quantities. One would expect that, if a chaotic system is sampled infrequently ($\tau\mu_1 \gg 1$), successive samples will be uncorrelated because of the growth of uncertainty between measurements. On the other hand, if the interval between successive samples is small ($\tau\mu_1 \ll 1$), one expects strong correlations between adjacent samples and a reduced entropy per sample. Experimental and theoretical work using semiconductor lasers has shown that these considerations are crucial to physical random number generation using chaotic dynamics (20, 21, 48). In the limit that $\tau, \varepsilon \to 0$, $h(\varepsilon, \tau)$ will approach a finite value, the Kolmogorov–Sinai (or metric) entropy, h_{ks} (40, 49–51). The metric entropy is related to the Lyapunov exponents, μ_i, by the following:

$$h_{ks} = \frac{1}{\log(2)} \sum_{\mu_i > 0} \mu_i. \qquad [5]$$

We calculated the spectrum of Lyapunov exponents from Eq. **1** (52, 53). There is only one positive Lyapunov exponent with a value of $\mu_1/\log(2) = 345$ bits/s. The Kaplan–Yorke dimension (54) calculated from the Lyapunov spectrum is 3.56.

The (ε, τ) entropy will have qualitatively different behavior as $\varepsilon \to 0$ depending on the physical origin of unpredictability. In chaotic systems, the entropy rate does not depend on either the sampling rate or the sampling resolution. This property of chaotic systems imposes a theoretical limitation on physical random number generation. Increasing the speed and resolution of a measurement device cannot in principle increase the entropy that can be harvested from a deterministic chaotic system beyond h_{ks}. In contrast to deterministic systems, the entropy rate of stochastic signals diverges like $-\log(\varepsilon)$ for finite τ (37, 39).

Another advantage of the (ε, τ) entropy is that it can be calculated from experimental data using an algorithm described by Cohen and Procaccia (55). In our case, we chose to calculate the entropy from $N_w(t)$ with a counting time window of $w = T_d/4$. With this window, $N_w(t)$ approximates the behavior of the deterministic signal $I(t)$ as seen in Figs. 2 and 3. We do not use an averaging time window to compute the entropy from deterministic simulations.

The first step to computing the entropy rate of an experimental signal is to generate a list of points in d-dimensional space using time delay embedding with a delay of τ. These vectors can be regarded as samples of a d-dimensional probability distribution over phase space. The entropy of this probability distribution, H_d, is sometimes referred to as the pattern entropy for patterns of length d (41). In principle H_d can be calculated by building a histogram with boxes of width ε and applying Shannon's formula, $H = -\sum_i p_i \log_2 p_i$ (56). In practice, direct application of this approach requires a very large amount of data when the embedding dimension is large. Cohen and Procaccia (55) proposed a more efficient algorithm to estimate the pattern entropy in the context of estimating metric entropy from experimental data. First, one randomly selects a small number M of reference points from the time series. In our case, $M = 5{,}000$ was sufficient. For each reference point i, one computes $n_i(\varepsilon)$, the fraction of points within a box of width ε centered on the reference point. The only difference between a direct calculation of the Shannon entropy and the Cohen–Procaccia procedure is that, in a direct calculation, a rectangular array of bins is used, rather than a set of bins centered on random points chosen from the dataset. In searching for neighbors for the ith reference point, we exclude points within a time window of τ of that point, as suggested by Theiler (57). The pattern entropy is then estimated by the following:

$$H_d(\varepsilon) = -\frac{1}{M} \sum_{i=1}^{M} \log_2 n_i(\varepsilon). \qquad [6]$$

It is a general feature of unpredictable signals that H_d grows linearly with d in the limit that d is large, and the entropy rate is the slope of this linear increase:

$$h(\varepsilon, \tau) = \frac{1}{\tau} \lim_{d \to \infty} [H_d(\varepsilon) - H_{d-1}(\varepsilon)]. \qquad [7]$$

Fig. 5 shows the entropy per unit time in both deterministic simulation and experiment with $\tau = (3/4)T_d$. The duration of the simulation was 512×10^6 T_d. Fig. 5*A* shows that, in the

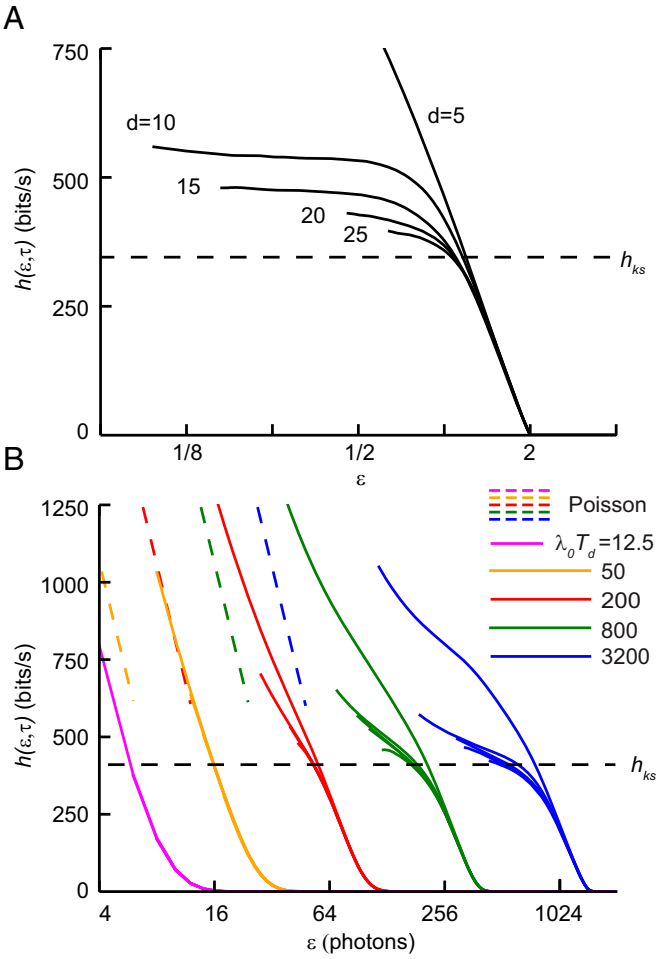

Fig. 5. (ε, τ) Entropy in deterministic simulation and experiment. Calculations with embedding dimensions of 5, 10, 15, 20, and 25 are shown. (*A*) Deterministic simulation. The entropy is calculated from the intensity, $I(t)$, which is normalized so that its values are between 1 (complete transmission through the modulator) and 0. ε is measured in the same units as $I(t)$. Characteristic of deterministic systems, the entropy rate is independent of ε and approaches the largest Lyapunov exponent as d increases. (*B*) Entropy rate of experimental time series. The entropy is calculated from $N_w(t)$, and ε is measured in photons. At low photon rates, we see a divergence characteristic of a Poisson processes. As the photon rate increases, the dependence of the entropy on ε becomes progressively flatter and approaches h_{ks}. Across photon rates, we see a divergence of the entropy rate for small ε. The Poisson curves were calculated by approximating the Shannon entropy of a Poisson process by an integral over a Gaussian distribution with a mean and variance of $\lambda_0 \bar{I} w$.

deterministic simulation, the entropy rate remains flat as ε decreases. As d increases, this plateau approaches h_{ks}, as indicated by Eq. **5**. In Fig. 5*B*, we see that, as the photon rate increases, the dependence of the entropy on ε becomes progressively flatter at high ε. Furthermore, in the region that this flattening is present, the value of $h(\varepsilon,\tau)$ is close to h_{ks}. The flattening of $h(\varepsilon,\tau)$ at high photon rate is another indication that this system behaves more deterministically in this regime. At all photon rates, we see $h(\varepsilon,\tau)$ sharply increases as ε decreases, which is due to the shot noise inherent in the system. It is natural to compare the entropy rates we observe to a constant-rate Poisson process with the same average rate. The Poisson curves in Fig. 5 were calculated by approximating the Shannon entropy of a Poisson distribution by an integral over a Gaussian distribution with a mean and variance of $\lambda_0\bar{I}w$. In the limit that $\varepsilon \ll \sqrt{\lambda_0\bar{I}w}$, this leads to the asymptotic expression $h(\varepsilon,\tau) = (-1/\tau)\log_2(\varepsilon/\sqrt{2\pi e\lambda_0\bar{I}w})$, indicated by the dashed curves in Fig. 5*B*. For small ε, $h(\varepsilon,\tau)$ increases logarithmically with decreasing ε, and parallels this curve. This logarithmic dependence is more pronounced at lower λ_0.

Discussion

We show in this paper that the choice of the resolution with which we observe our system allows us to see either noisy or deterministic dynamics. By counting photon arrivals over timescales on the order of the delay time and filter time constants, we see deterministic dynamics in the time series, Poincaré sections, and the autocorrelation functions. Furthermore, when we observe the dynamics on large scales of both value (ε) and time (w and τ), we find that the entropy rate is close in value to the metric entropy calculated from the positive Lyapunov exponents of the deterministic model, which shows that the entropy generation is dominated by the deterministic exponential amplification of small perturbations in this regime.

In contrast, by using high resolution in photon counts and timescales, we see that both the entropy rate and variance reflect the stochastic nature of the photon arrivals. For small values of w, the variance of the number of photon counts is equal to the average number of counts, characteristic of a Poisson process. The logarithmic dependence of the entropy on ε shown in Fig. 5 offers another indication of the noisy nature of the dynamics at small scales. In addition to showing both shot noise and chaos at different scales, our experiment also shows a transition from shot noise to chaos with increasing photon rate. The precise control over the rate of photon arrivals and dynamical timescales afforded by our experiment allows for experimental observation of the interplay of noise and dynamics. Our results can be seen to bridge two widely used methods of physical random number generation.

Two prevalent methods have attracted attention for optical random number generation: those based on single-photon detection from strongly attenuated light sources (58, 59), and those based on digitized high-speed fluctuations from chaotic lasers (13). In the former case, the entropy is claimed to originate entirely from quantum mechanical uncertainty, yet in practice these methods are also subject to unpredictable drift and environmental variations. In the latter case, the entropy is attributed to the dynamical unpredictability of chaos, but the unavoidable presence of spontaneous emission is thought to play a role in seeding these macroscopic fluctuations (20, 21). The system presented here is unprecedented in that it can approach macroscopic chaos from the single-photon limit, thereby revealing the transition from noise to chaos. Moreover, the analysis offers a unified measure of entropy that captures both behaviors and clarifies the relationship between sampling frequency, measurement resolution, and entropy rate.

The designer of a physical random number generator must choose the sampling rate and resolution that they will use to collect numbers from a physical system. These decisions will impact the entropy rate. Heuristically, finer discretization (smaller ε) and more frequent sampling (smaller τ) lead to higher entropy rates, but without the methods presented here it is difficult to assess the dependence of the entropy rate on these parameters in any given system. The statistical tests that are usually used to evaluate physical random number generation (26, 27) were not designed to answer these questions, but rather to certify that a stream of bits is free of bias and correlation. If a random number generator employs postprocessing (as most do), existing statistical tests applied to the output binary sequence provide no insight into whether the entropy originates from the physical process or the postprocessing algorithm used. The (ε, τ) entropy clarifies the origin and nature of uncertainty and informs the choice of sampling rate and measurement resolution.

ACKNOWLEDGMENTS. We acknowledge the University of Maryland supercomputing resources (it.umd.edu/hpcc) made available in conducting the research reported in this paper. We gratefully acknowledge Grant N000141410443 from the Office of Naval Research.

1. Bialek W (2012) *Biophysics: Searching for Principles* (Princeton Univ Press, Princeton).
2. Izhikevich EM, Edelman GM (2008) Large-scale model of mammalian thalamocortical systems. *Proc Natl Acad Sci USA* 105(9):3593–3598.
3. May RM (2001) *Stability and Complexity in Model Ecosystems* (Princeton Univ Press, Princeton), Vol 6.
4. Chowdhury D, Santen L, Schadschneider A (2000) Statistical physics of vehicular traffic and some related systems. *Phys Rep* 329(4):199–329.
5. Mantegna RN, Stanley HE (1999) *Introduction to Econophysics: Correlations and Complexity in Finance* (Cambridge Univ Press, Cambridge, UK).
6. Preis T, Schneider JJ, Stanley HE (2011) Switching processes in financial markets. *Proc Natl Acad Sci USA* 108(19):7674–7678.
7. Anderson RM, May RM (1991) *Infectious Diseases of Humans* (Oxford Univ Press, Oxford), Vol 1.
8. Mandel L, Wolf E (1995) *Optical Coherence and Quantum Optics* (Cambridge Univ Press, Cambridge, UK).
9. Benzi R, Sutera A, Vulpiani A (1981) The mechanism of stochastic resonance. *Journal of Physics A: Mathematical and General* 14(11):L453.
10. Pikovsky AS, Kurths J (1997) Coherence resonance in a noise-driven excitable system. *Phys Rev Lett* 78(5):775.
11. Lenstra A, et al. (2012) Ron was wrong, Whit is right (IACR ePrint Archive), Technical Report 2012/064.
12. Hamburg M, Kocher P, Marson ME (2012) Analysis of intels ivy bridge digital random number generator. Available at www.cryptography.com/public/pdf/Intel_TRNG_Report_20120312.pdf. Accessed July 2, 2015.
13. Uchida A, et al. (2008) Fast physical random bit generation with chaotic semiconductor lasers. *Nat Photonics* 2(12):728–732.
14. Yamazaki T, Uchida A (2013) Performance of random number generators using noise-based superluminescent diode and chaos-based semiconductor lasers. *IEEE J Sel Top Quantum Electron* 19(4):0600309.
15. Sakuraba R, Iwakawa K, Kanno K, Uchida A (2015) Tb/s physical random bit generation with bandwidth-enhanced chaos in three-cascaded semiconductor lasers. *Opt Express* 23(2):1470–1490.
16. Li X, Cohen AB, Murphy TE, Roy R (2011) Scalable parallel physical random number generator based on a superluminescent LED. *Opt Lett* 36(6):1020–1022.
17. Williams CRS, Salevan JC, Li X, Roy R, Murphy TE (2010) Fast physical random number generator using amplified spontaneous emission. *Opt Express* 18(23):23584–23597.
18. Rosin DP, Rontani D, Gauthier DJ (2013) Ultrafast physical generation of random numbers using hybrid Boolean networks. *Phys Rev E Stat Nonlin Soft Matter Phys* 87(4):040902.
19. Kanter I, Aviad Y, Reidler I, Cohen E, Rosenbluh M (2009) An optical ultrafast random bit generator. *Nat Photonics* 4(1):58–61.
20. Harayama T, et al. (2012) Theory of fast nondeterministic physical random-bit generation with chaotic lasers. *Phys Rev E Stat Nonlin Soft Matter Phys* 85(4 Pt 2):046215.
21. Sunada S, et al. (2012) Noise amplification by chaotic dynamics in a delayed feedback laser system and its application to nondeterministic random bit generation. *Chaos* 22(4):047513.
22. Oliver N, Soriano MC, Sukow DW, Fischer I (2011) Dynamics of a semiconductor laser with polarization-rotated feedback and its utilization for random bit generation. *Opt Lett* 36(23):4632–4634.
23. Oliver N, Cornelles Soriano M, Sukow DW, Fischer I (2013) Fast random bit generation using a chaotic laser: Approaching the information theoretic limit. *IEEE J Quantum Electron* 49(11):910–918.
24. Virte M, Mercier E, Thienpont H, Panajotov K, Sciamanna M (2014) Physical random bit generation from chaotic solitary laser diode. *Opt Express* 22(14):17271–17280.
25. Gabriel C, et al. (2010) A generator for unique quantum random numbers based on vacuum states. *Nat Photonics* 4(10):711–715.

26. Rukhin A, et al. (2001) A statistical test suite for random and pseudorandom number generators for cryptographic applications (National Institute of Standards and Technology, Gaithersburg, MD), NIST Special Publication 800-22.
27. Marsaglia G (1998) DIEHARD Test suite. Available at www.stat.fsu.edu/pub/diehard/. Accessed August 1, 2014.
28. Barker E, Kelsey J (2012) Recommendation for the entropy sources used for random bit generation (National Institute of Standards and Technology, Gaithersburg, MD), NIST DRAFT Special Publication 800-90b.
29. Bérut A, et al. (2012) Experimental verification of Landauer's principle linking information and thermodynamics. *Nature* 483(7388):187–189.
30. Sethna J (2006) *Statistical Mechanics: Entropy, Order Parameters, and Complexity* (Oxford Univ Press, Oxford), Vol 14.
31. Jarzynski C (2015) Diverse phenomena, common themes. *Nat Phys* 11(2):105–107.
32. Touchette H (2009) The large deviation approach to statistical mechanics. *Phys Rep* 478(1):1–69.
33. Roldán E, Parrondo JMR (2010) Estimating dissipation from single stationary trajectories. *Phys Rev Lett* 105(15):150607.
34. Andrieux D, et al. (2007) Entropy production and time asymmetry in nonequilibrium fluctuations. *Phys Rev Lett* 98(15):150601.
35. Andrieux D, et al. (2008) Thermodynamic time asymmetry in non-equilibrium fluctuations. *J Stat Mech* 2008(01):P01002.
36. Caputo JG, Atten P (1987) Metric entropy: An experimental means for characterizing and quantifying chaos. *Phys Rev A* 35(3):1311–1316.
37. Gaspard P, Wang XJ (1993) Noise, chaos, and (ε, τ)-entropy per unit time. *Phys Rep* 235(6):291–343.
38. Dettmann CP, Cohen EGD, van Beijeren H (1999) Statistical mechanics: Microscopic chaos from Brownian motion? *Nature* 401(6756):875.
39. Cencini M, Falcioni M, Olbrich E, Kantz H, Vulpiani A (2000) Chaos or noise: Difficulties of a distinction. *Phys Rev E Stat Phys Plasmas Fluids Relat Interdiscip Topics* 62(1 Pt A): 427–437.
40. Boffetta G, Cencini M, Falcioni M, Vulpiani A (2002) Predictability: A way to characterize complexity. *Phys Rep* 356(6):367–474.
41. Gaspard P, et al. (1998) Experimental evidence for microscopic chaos. *Nature* 394(6696): 865–868.
42. Briggs M, et al. (2001) Tracking a colloidal particle for the measurement of dynamic entropies. *Physica A* 296(1):42–59.
43. Peil M, Jacquot M, Chembo YK, Larger L, Erneux T (2009) Routes to chaos and multiple time scale dynamics in broadband bandpass nonlinear delay electro-optic oscillators. *Phys Rev E Stat Nonlin Soft Matter Phys* 79(2 Pt 2):026208.
44. Murphy TE, et al. (2010) Complex dynamics and synchronization of delayed-feedback nonlinear oscillators. *Philos Trans A Math Phys Eng Sci* 368(1911):343–366.
45. Larger L (2013) Complexity in electro-optic delay dynamics: Modelling, design and applications. *Philos Trans A Math Phys Eng Sci* 371(1999):20120464.
46. Williams CRS, et al. (2013) Experimental observations of group synchrony in a system of chaotic optoelectronic oscillators. *Phys Rev Lett* 110(6):064104.
47. Kouomou YC, Colet P, Larger L, Gastaud N (2005) Chaotic breathers in delayed electro-optical systems. *Phys Rev Lett* 95(20):203903.
48. Mikami T, et al. (2012) Estimation of entropy rate in a fast physical random-bit generator using a chaotic semiconductor laser with intrinsic noise. *Phys Rev E Stat Nonlin Soft Matter Phys* 85(1 Pt 2):016211.
49. Pesin YB (1977) Characteristic Lyapunov exponents and smooth ergodic theory. *Russ Math Surv* 32(4):55–114.
50. Eckmann JP, Ruelle D (1985) Ergodic theory of chaos and strange attractors. *Rev Mod Phys* 57(3):617–656.
51. Benettin G, Galgani L, Strelcyn JM (1976) Kolmogorov entropy and numerical experiments. *Phys Rev A* 14(6):2338–2345.
52. Farmer JD (1982) Chaotic attractors of an infinite-dimensional dynamical system. *Physica D* 4(3):366–393.
53. Geist K, Parlitz U, Lauterborn W (1990) Comparison of different methods for computing Lyapunov exponents. *Prog Theor Phys* 83(5):875–893.
54. Grassberger P, Procaccia I (1983) Measuring the strangeness of strange attractors. *Physica D* 9:189–208.
55. Cohen A, Procaccia I (1985) Computing the Kolmogorov entropy from time signals of dissipative and conservative dynamical systems. *Phys Rev A* 31(3):1872–1882.
56. Cover TM, Thomas JA (2012) *Elements of Information Theory* (Wiley, Hoboken, NJ), Chap 4.
57. Theiler J (1990) Estimating fractal dimension. *JOSA A* 7(6):1055–1073.
58. Jennewein T, Achleitner U, Weihs G, Weinfurter H, Zeilinger A (2000) A fast and compact quantum random number generator. *Rev Sci Instrum* 71(4):1675–1680.
59. Dynes JF, Yuan ZL, Sharpe AW, Shields AJ (2008) A high speed, postprocessing free, quantum random number generator. *Appl Phys Lett* 93(3):031109.